Power-law fluid flow around a triangular cylinder in laminar flow regime

Thesis submitted to the

National Institute of Technology Rourkela

in partial fulfillment of the necessity

of the degree of

Bachelor of Technology

in

Chemical Engineering

by

Ashis Kumar

(Roll No: 112CH0079)

under the supervision of

Prof. Akhilesh Kumar Sahu

May, 2016

Department of Chemical Engineering

National Institute of Technology Rourkela

Department of Chemical Engineering
National Institute of Technology Rourkela

Prof. Akhilesh Kumar Sahu
Assistant Professor

May 12, 2016

Supervisor's Certificate

This is to certify that the work presented in this dissertation entitled "*Power-law fluid flow around a triangular cylinder in laminar flow regime*" by "*Ashis Kumar*", Roll Number 112CH0079, is a record of research carried out by him under my supervision and guidance in partial fulfillment of the requirements of the degree of *Bachelor of Technology* in *Chemical Engineering*.

Akhilesh Kumar Sahu

ACKNOWLEDGEMENT

I would like to express my heartfelt gratitude to Prof. Akhilesh Kumar Sahu, my project supervisor, for his indispensable help, relentless and unshakeable encouragement throughout my work. Being able to do this project under him, helped me to enhance my knowledge in the fields of “Computational Fluid Dynamics “.

I would like to thank all our professors who helped me explore many new frontiers of knowledge. I am grateful to my friends Siddhartha, Swetashree, Vikash for helping me out and making my problems easier to solve.

Last but not the least, love, blessings and best wishes of my parents and siblings had been a persistent source of inspiration and encouragement throughout my entire project work.

May 12, 2016 *Ashis Kumar*

NIT ROURKELA Roll Number: 112CH0079

ABSTRACT

Fluid flow past triangular cylinder in 2D has been scrutinized numerically by solving continuity equations and momentum equations in ANSYS FLUENT (version 15), in steady laminar flow regime. The effect of the Reynolds number ($10 \leq Re \leq 40$), in case of Power-law fluid, on the local and global flow characteristics has been investigated. In addition, flow orientations showing streamlines, recirculation length and the pressure variation on the surface of the cylinder have also been observed in order to provide further physical capacity to gain an accurate and deep understanding of the detailed flow kinematics. The pressure coefficient, total drag coefficient and recirculation length, show a relatively complex dependence on the Reynolds number.

Keywords: Power-law fluid; Reynolds number; Drag coefficient; Streamline; Recirculation length; Laminar flow

Contents

List of Figures

List of Tables

Nomenclature

b	-	Side of the triangular cylinder, m
C_D	-	Drag coefficient coefficient
C_{DP}	-	Pressure drag coefficient
L_R	-	Recirculation Length, m
F_D	-	Drag force per unit length of cylinder (N/m)
I_2	-	Second invariant of the rate of strain tensor
m	-	Power-law consistency index (Pa s^n)
n	-	Power-law index
P, p	-	Pressure (Pa)
Re	-	Reynolds number
u,v	-	Velocity (m/s)
U_x	-	x-velocity (m/s)
U_y	-	y-velocity (m/s)
U_∞, U_0	-	Uniform velocity of fluid at inlet (m/s)

Greek letters

ε	=	Rate of strain tensor
ρ	=	Density (kg/m^3)
τ	=	Shear stress
μ, η	=	Dynamic viscosity (Pa s)

Chapter 1

Introduction

Flow past bluff bodies is an intense topic of research since last 100 years because of its applications with engineering significance. Electronic cooling, structural design, heat exchanger systems, acoustic emission are a few to name. It also embraces a huge deal of academic interest owing to a range of fluid mechanical issues it presents. Recently, it has gained attention in terms of both numerical and experimental studies, as result of increasing computational power and advent of new experimental phenomena and methods.

There are numerous number of fluids such as gases like air and most simple liquids like water that exhibit Newtonian characteristic behaviors, which are characterized by dynamic viscosity, mathematically defined as shear stress divided by corresponding shear rate, which doesn't change with the shear rate. Perhaps on the other hand, it is readily appreciated that many structured fluids of micro-molecular nature and multiple phase systems that we come across in industrial practice, exhibit flow properties which are dissimilar enough to Newtonian fluids. Accordingly, such fluids are variously known as non-Newtonian or nonlinear or rheologically complex fluids. Even though non-Newtonian fluid behaviors can be differentiated in several ways, most of these systems show the so called shear-thinning behavior. This can be characterized by an apparent viscosity, that is defined as shear stress divided by the corresponding shear rate, and hence it decreases with the increasing shear rate. Counter to this behavior is the behavior of shear thickening fluids, whose apparent viscosity increase with the increasing shear rate. Most suspensions, emulsions, polymeric systems, and foams display shear-thinning behavior under certain suitable conditions. On the other hand, few dense pastes and suspensions exhibit the shear-thickening fluid behavior.

Power-law fluid is a type of generalized fluid for which the shear stress τ is given by,

$$\boldsymbol{\tau} = 2\boldsymbol{\eta}\boldsymbol{\varepsilon}(\boldsymbol{u}) \tag{1.1}$$

Where ε(u) is the component of the rate of strain tensor, and is given by,

$$\boldsymbol{\varepsilon}(\boldsymbol{u}) = \frac{1}{2}\{(\boldsymbol{\nabla u}) + (\boldsymbol{\nabla u})^T\} \tag{1.2}$$

The viscosity, η, is given by

$$\boldsymbol{\eta} = m\left(\frac{\boldsymbol{I}_2}{2}\right)^{(n-1)/2} \tag{1.3}$$

where m represents the power-law consistency index and n represents the power-law index of the fluid; and I_2 is the second invariant of the rate of strain tensor ($\boldsymbol{\varepsilon}$), given by

$$\boldsymbol{I}_2 = \left(\varepsilon_{xx}^2 + \varepsilon_{yy}^2\right) + \left(\varepsilon_{xy}^2 + \varepsilon_{yx}^2\right) \tag{1.4}$$

and the components of the rate of strain tensor can be related to the velocity components as follows

$$\varepsilon_{xx} = \frac{\partial U_x}{\partial x}, \quad \varepsilon_{yy} = \frac{\partial U_y}{\partial y}, \quad \varepsilon_{xy} = \varepsilon_{yx} = \frac{1}{2}\left(\frac{\partial U_x}{\partial y} + \frac{\partial U_y}{\partial x}\right) \tag{1.5}$$

In fluid dynamics, drag (sometimes called a type of friction, known as air resistance, or another type of friction or fluid friction, known as fluid resistance) is a force acting opposite to or opposing the relative motion of any body mass moving with respect to a surrounding fluid. This can be seen between two fluid layers, or two surfaces, or a fluid and a solid surface. Unlike other resistance forces, such as dry friction, which are almost independent of velocity, drag forces depend on velocity. For a laminar flow drag force is proportional to the velocity while for a turbulent flow, drag is proportional to the squared velocity. Even though the ultimate cause of a drag is viscous friction, the turbulent drag is independent of viscosity.

$$\mathrm{F_D} = \frac{1}{2}\rho v^2 C_D A \tag{1.6}$$

The drag force basically possesses two components: frictional drag and pressure drag. Frictional drag comes from friction acting between the fluid and the surface of the body over which it is flowing. This friction is responsible for the development of boundary layers. Pressure drag originates from the eddying motions which are setup in the fluid by the motion of the body. This drag is always associated with the separation in the fluid flow or formation of wake, and it is usually less sensitive to Reynolds number as compared to the frictional drag.

1.1 Triangular Cylinder

For an equilateral triangular cylinder placed in a fluid flow stream, the orientation further affects the transition, e.g., whether the apex is facing upstream or downstream direction. There has been a very less work on the calculation of critical Reynolds number, even in Newtonian fluids.

Furthermore, not all researchers have reported the criterion used by them to delineate the value of the critical Reynolds number, distinct onset of the vortex shedding, lift coefficient, etc. Values of the critical Reynolds number are more likely to differ somewhat from one criterion to the other.

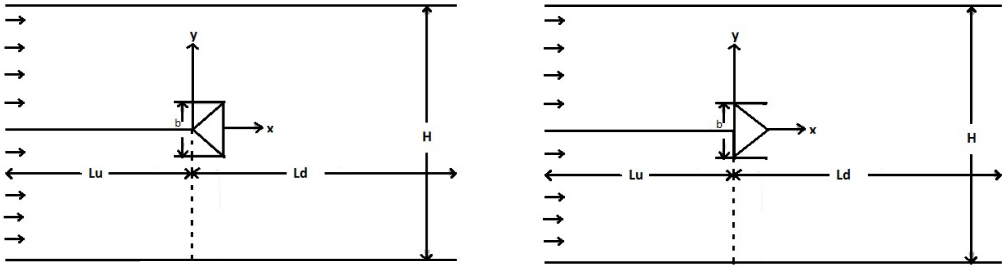

Fig.1.1: Schematics of the computational geometry

1.2 Flow Regimes

The flow is seen to be attached to the surface of the cylinder at lower Reynolds number, whereas it is known to have detached itself at high Reynolds number, thereby suggesting the value of Re_c to lie in between this interval. Evidently, the differences in the values of Re_c for the two configurations arise from the reduced degree of streamlining in case of the vertex oriented in the upstream

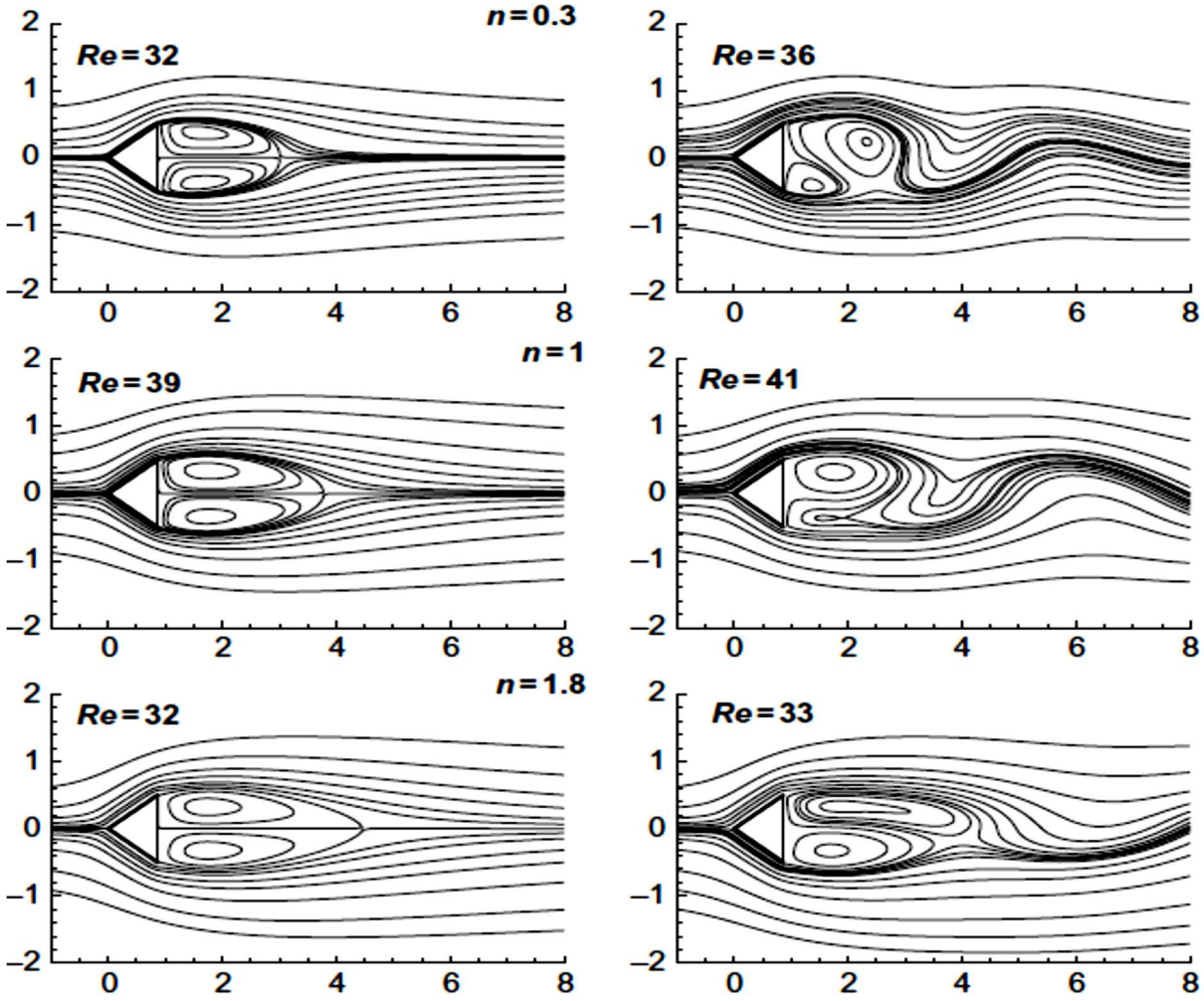

Fig. 1.2. Representative instantaneous streamline contours showing the initiation of vortex shedding regime for an equilateral triangular cylinder with vertex facing upstream[6].

direction. Contrariwise, because of the sudden extremity of the rear surface, the fluid element is prevented from negotiating such an abrupt change in direction which causes the flow to detach.

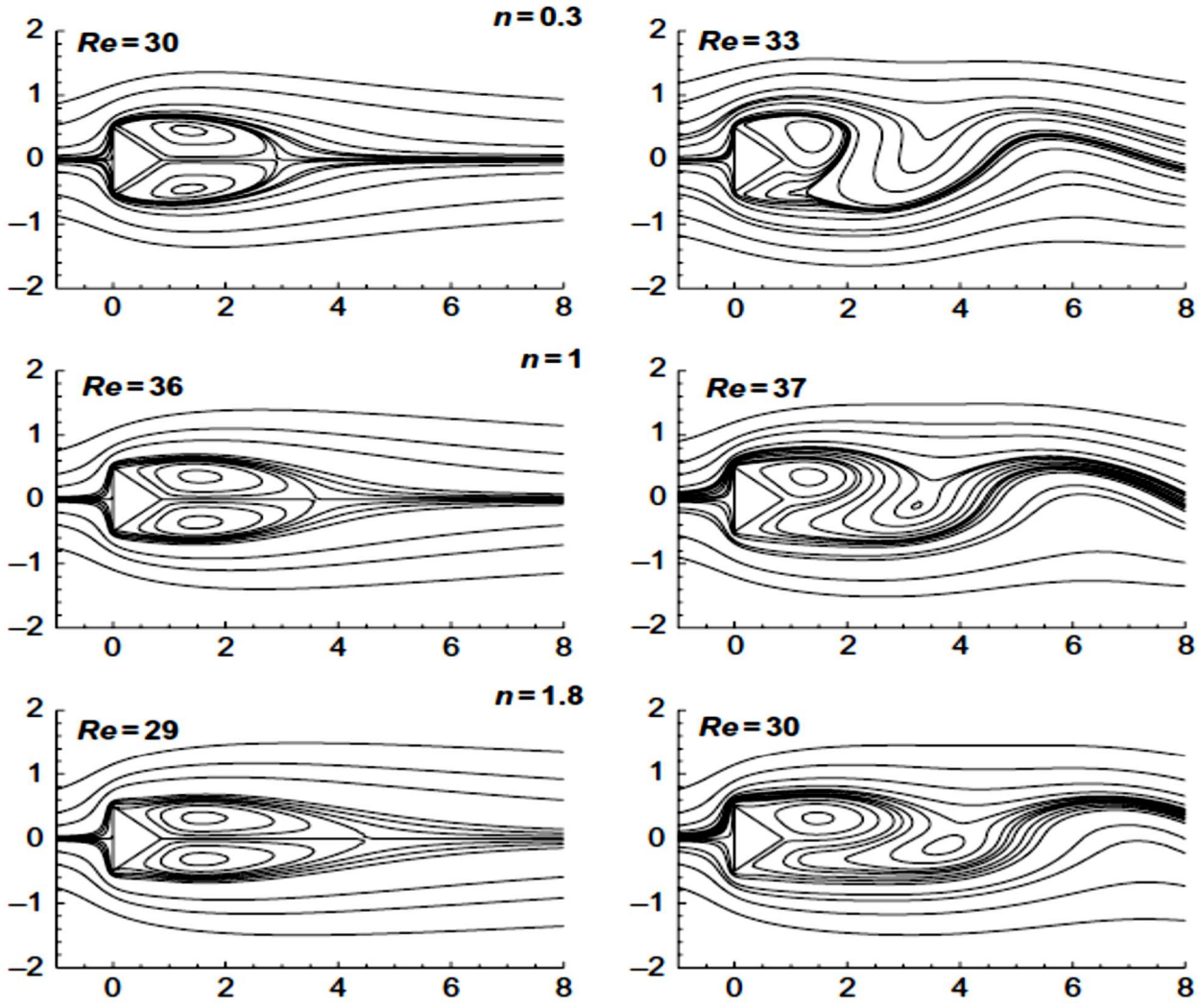

Fig. 1.3. Representative instantaneous streamline contours showing the initiation of vortex shedding regime for an equilateral triangular cylinder with vertex facing downstream[6].

Chapter 2

Literature Review

This section presents the review of the previous work related to the current investigation. There have been a few studies on the two-dimensional flow past cylinders of triangular cross section, but their major thrust has been on elucidating the momentum and heat transfer characteristics under various conditions of orientation, incarcerated or unrestrained, forced and mixed convection regimes, etc. The Reynolds number in all the literature cited are based on the edge length of the triangular cylinders.

Jackson[3], *De and Dalal*[6], *Zielinska and Wesfreid*[4] all examined numerically the transformation from steady to time-dependent flow past a triangular cylinder (with vertex aligned along with the direction of the oncoming flow) incarcerated in a planar channel (with a blockage ratio of 1/15) and reported a value of Re^c(critical reynolds number) in the range $\sim 36.4\ to\ \sim 40$.

Abbassi et al.[5] investigated flow and heat transfer characteristics around a triangular prism with a base to height ratio of 0.5, incarcerated in a planar channel (with a blockage ratio of 1/4). They reported the wake to lose its symmetry at $Re = 45$ which was also consistent with the basic conception that the confinement possesses a tendency to stabilize the flow, although more recent research suggests this value to be in the vicinage of $Re = 58 - 59$.

Faruquee and Olatunji[7] studied the unrestrained flow around a two dimensional triangular cylinder for its vertex facing/opposing the flow, in the range of Reynolds number $30 \leq Re \leq 150$. They reported the value of critical Reynolds number to be in the range $40 \leq Re \leq 42$ for both the orientations, which is larger to some extent than the previous values. However, it is suitable to add here that it is not at all unusual to obtain deviations of such order because of the differences in grid, domain, solution methodology, convergence criterion, etc.

Srikanth et al.[8] have investigated how the symmetric planar confinement affects drag and heat transfer parameters for a triangular cylinder with its apex oriented upstream direction, in the range of Reynolds number $1 \leq Re \leq 80$, and for a single Prandtl number value of 0.71 and for a constant blockage ratio of (1/4). They discussed the effect of confinement as more dramatic for the time-dependent flow regime as compared to that in steady flow regime.

$Prhashanna\ et\ al.$[9] have comprehensibly investigated how the power-law index affects heat transfer around an isothermal-equilateral triangular cylinder when its vertex faces upstream or downstream. So along as this study is restrained to the so-known steady flow regime ($Re \leq 30$), it does cover wide range of values of the power-law index ($0.2 \leq n \leq 1$) as well as Prandtl number ($1 \leq Pr \leq 100$).

The present work focuses on calculating the flow characteristics for Power-law fluids past a triangular cylinder kept in a laminar flow regime. The velocity field in the flow domain is obtained by solving the continuity and momentum equation using FLUENT (version 15). The range of Reynolds number investigated is from 10 to 40 and the power-law indices used for the fluids used is 0.2, 1 and 1.8. The velocity profiles are used to investigate the total drag force and pressure drag force on the triangular cylinder. The effect of the Reynolds number and power-law index on total drag coefficient, pressure drag coefficient, streamlines and recirculation length has been studied and validated with the literature.

Chapter 3

Mathematical Formulation

3.1 Governing Equations

Continuity equation:

$$\boldsymbol{\nabla u} = 0 \tag{3.1}$$

Momentum equation:

$$\rho(u.\boldsymbol{\nabla u} - f) - \boldsymbol{\nabla}.\sigma = 0 \tag{3.2}$$

where $\rho, \boldsymbol{u}, \boldsymbol{f}$ and σ are the density, velocity, body force and stress tensor respectively.

3.2 Boundary Conditions

The physically reasonable boundary conditions for this flow can be composed as follows:

- At the inlet boundary, uniform flow in the x- direction is endorsed, i.e.,

$$U_x = U_\infty \; ; \; U_y = 0 \tag{3.3}$$

- Walls of the triangular cylinder: No-slip boundary i.e.,

$$U_x = 0 \; ; \; U_y = 0 \tag{3.4}$$

- At the outlet-boundary: The pressure outlet boundary condition which is by default set in FLUENT is used and it assumes a zero diffusive flux for all flow variables, and this is the same as that of the fully evolved flow condition.

- The top and bottom walls are taken to be slip boundaries, i.e.,

$$U_x = 0 \; ; \; \frac{dU_x}{dy} = 0 \tag{3.5}$$

3.3 Numerical Methodology

The present study has been carried out using ANSYS FLUENT (version 15). Multizone triangular and quadrilateral cells of uniform grid spacing were generated using the FLUENT software. The continuity and momentum equations were solved with the use of Semi-Implicit Method for Pressure Linked Equations (SIMPLE) method. The physical properties of the fluid were input with the use of constant density and non-newtonian power-law viscosity models ($Re = \frac{\rho v^{2-n} D^n}{\mu}$). This, however, has no particular significance as the final results are represented in the form of dimensionless quantities. The relative convergence criteria of 10^{-8} for the continuity and x- and y-components of the momentum equations were prescribed in this work. Also, the solution was deemed to have converged when there was no change (at least up to the fourth decimal place) in the value of the total drag coefficient.

3.4 Grid Independence Test

A number of grids were generated to obtain an optimal grid that would be accurate enough, without any excessive consumption of computational resources such as of CPU time and memory. While a range of composite grids consisting of multizone triangular/quadrilateral cells were generated in this work. A minimum mesh size of $\delta = 0.003b$ has been used over a separation of $3b$ in both x and y-directions surrounding the triangular cylinder, and the grid was constructed progressively coarse by using a successive growth rate of 1.03. For instance, at Re = 10, unstructured quadrilateral grid has been used. The total number of cells on the surface of the triangular cylinder ranged from $60\ to\ 300$ where as the total number of cells ranged from ~30,000 to ~1,00,000.

Table 3.1: Values of C_D and C_{DP} for different grids, for vertex facing upstream

Grids	*No. of Cells*	N_P	C_D			C_{DP}		
			n=0.2	*n=1*	*n=1.8*	*n=0.2*	*n=1*	*n=1.8*
G1	33457	75	2.8992	2.7953	2.6741	2.2409	1.4551	1.1325
G2	50494	150	2.8997	2.7971	2.6758	2.2419	1.464	1.1431
G3	81469	300	2.9002	2.7986	2.6772	2.243	1.4719	1.1524

Table 3.2: Values of C_D and C_{DP} for different grids, for vertex facing downstream

Grid	*No. of Cells*	N_P	C_D			C_{DP}		
			n=0.2	*n=1*	*n=1.8*	*n=0.2*	*n=1*	*n=1.8*
G1	47085	60	3.0498	2.7979	2.6729	2.7671	2.4349	2.2668
G2	65805	120	3.0562	2.8083	2.6809	2.8113	2.5094	2.4455
G3	94866	240	3.0621	2.8137	2.6852	2.8402	2.5607	2.4039

Tables 3.1 and 3.2 summarize the results demonstrating the effect of grid size, for the vertex of the triangular cylinder facing upstream and downstream respectively. A brief study of the tables suggest that G1 is sufficient for each of the orientations. It needs to be stressed here that G1 is only symbolic because it varied negligibly from one case to the other. While the pressure drag coefficient and the total drag coefficient rarely change by more than ∼0.5% in moving on from Grid G1 to G2. Hence, the grid G1 was ultimately used for this work in the steady laminar flow regime.

Chapter 4

Results and Discussion

4.1 Square Cavity

Fig. 4.1 shows the streamline contours for the traditional square cavity flow problem, for the Reynolds number 100, 400 and 1000. The extent of various secondary vortices obtained are in excellent agreement with the ones reported by Ghia et al[2].

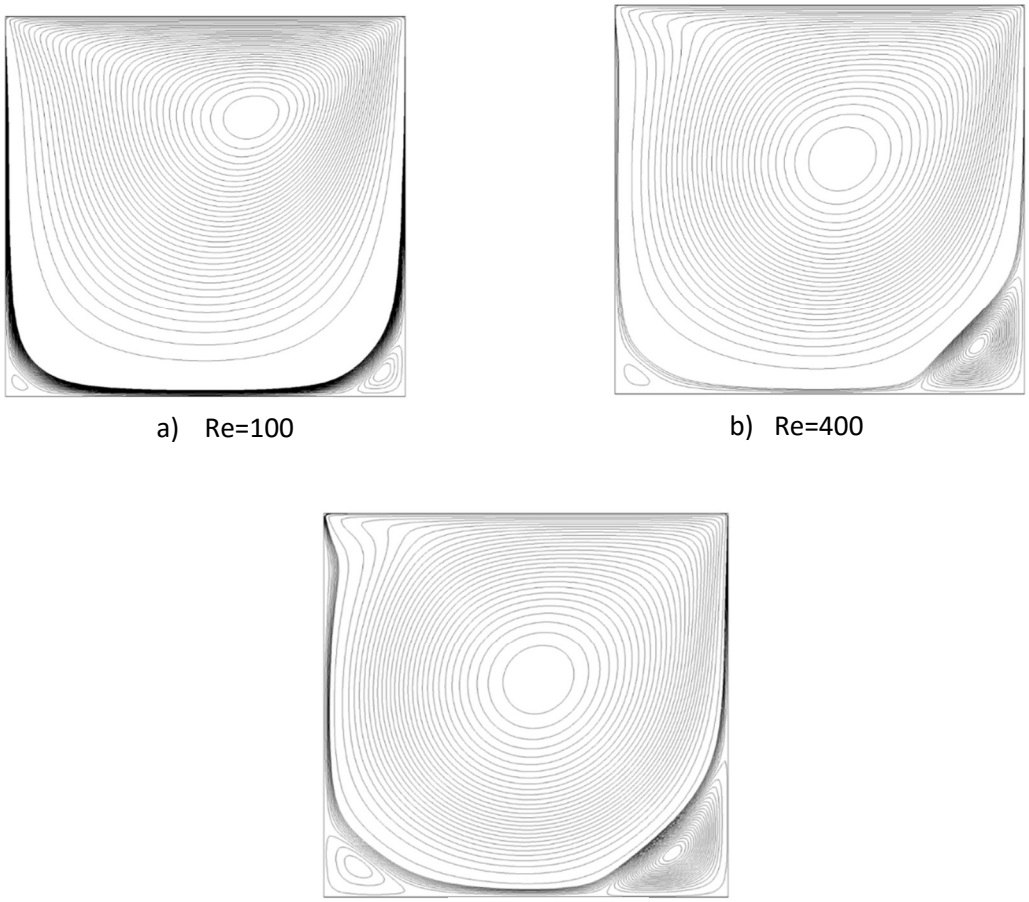

a) Re=100

b) Re=400

c) Re=1000

Fig. 4.1. Streamline patterns inside the cavity

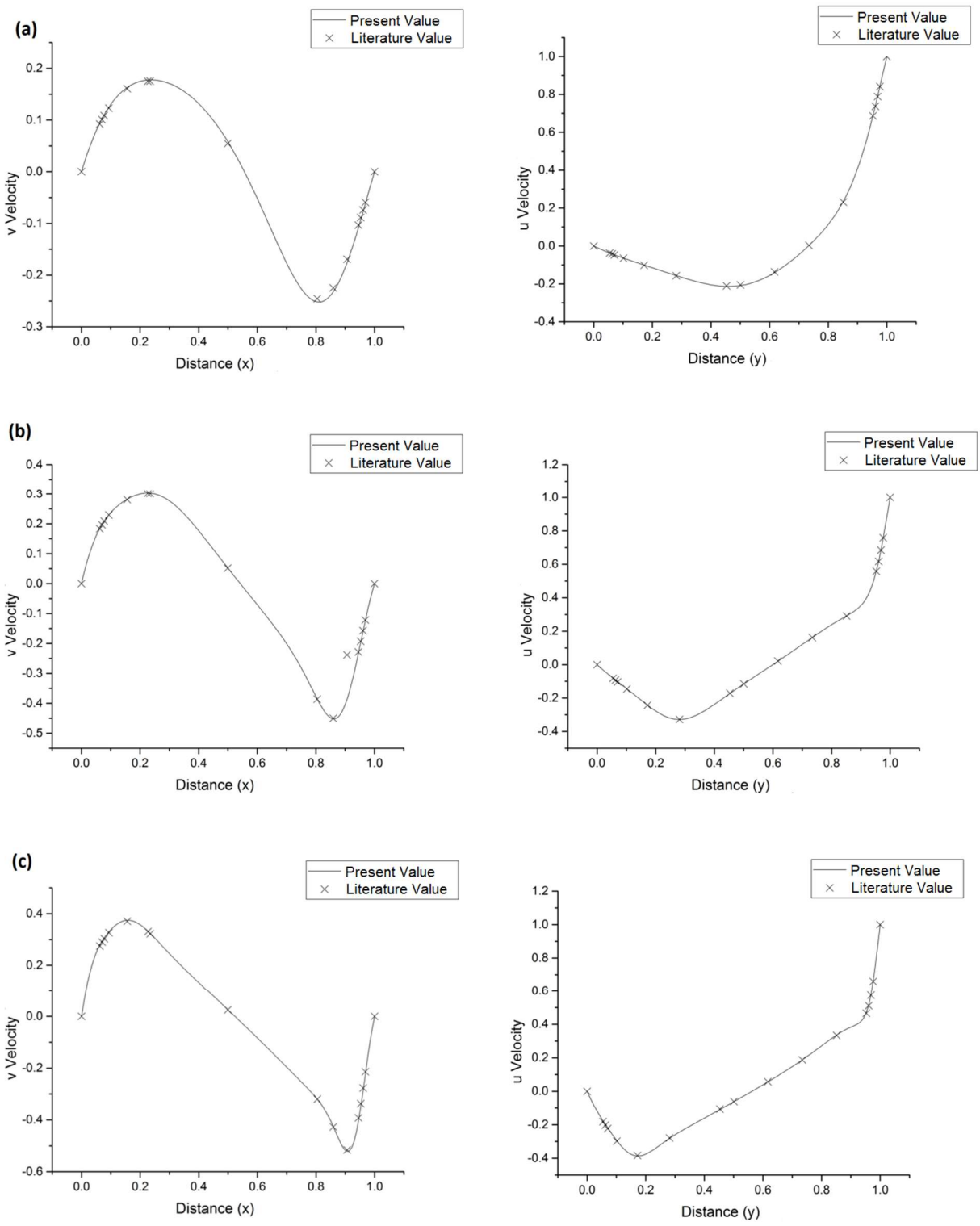

Fig. 4.2. X-velocity and Y-velocity plot along the vertical and horizontal axes of the cavity respectively, for a) Re=100, b) Re=400 & c) Re=1000

Much efficient fine mesh solutions were obtained, using ANSYS FLUENT. The finest mesh element employed in the grid pattern, is considered to be a parameter of much significance.

The sturdiness in construction and the efficiency of the overall solution method has been validated using the model problem of lid driven square cavity. The present results are in well agreement with the literature of multigrid solutions.

As the Re value increases, various regions of higher vorticity gradients, denoted by concentration of vorticity contours, are found to appear inside the cavity. Fig. 4.1 clearly elucidates that these regions of high vorticity gradients are not aligned along the geometric boundaries of the square cavity. It is because of these reasons, that a uniform structured mesh refinement was considered in the present study. As can be seen from Fig. 4.1, fine mesh solutions are able to show additional counter recirculating vortices inside or near the corners of the cavity, as Re increases. It is also observed that Re affects the position of the geometric centers of the vortices. As the Re value increases, the primary vortex is displaced in a direction approaching the center of the cavity.

4.2 Triangular Cylinder

In this work steady flow computations have been carried out for both, vertex facing upstream and downstream. The results presented here, for the vertex facing upstream, are based on the domain size 37×40 for Power-law indices 0.2, 1 and 1.8, and Re =10, 20, 25, 30 and 40. And for vertex facing downstream, The results presented here, for the vertex facing downstream, are based on the domain size 50×70 for Power-law indices 0.2, 1 and 1.8, and Re =10, 20, 25, 30 and 40, and the grid near the cylinder is sufficiently refined to resolve the boundary conditions.

4.2.1 Vertex Facing Upstream

a)

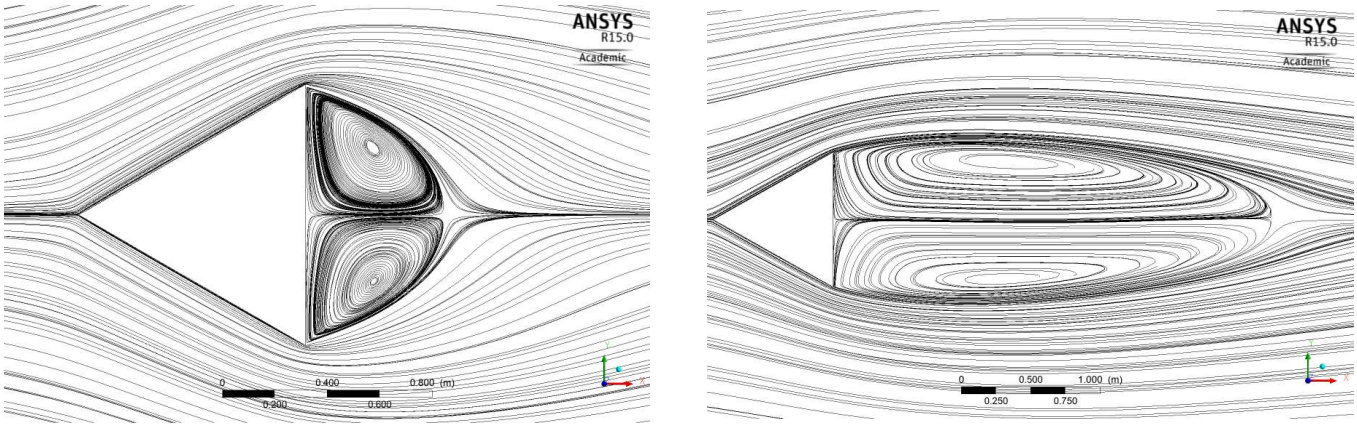

Fig. 4.3. Streamline patterns, in case of vertex facing upstream, for Reynolds number 10(left) and 40(right), and power-law index; a) n=0.2, b) n=1, c) n=1.8.

b)

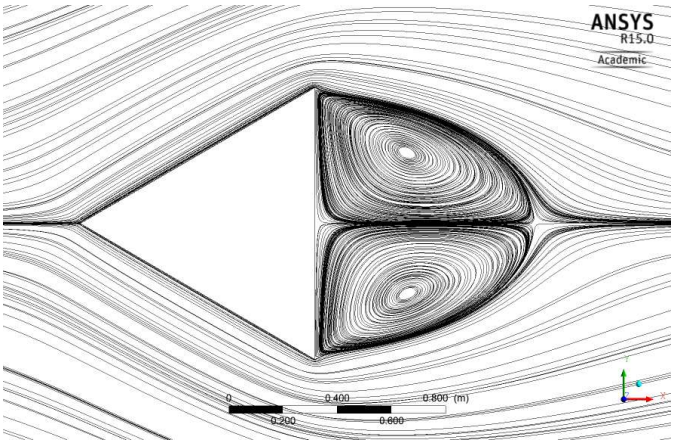

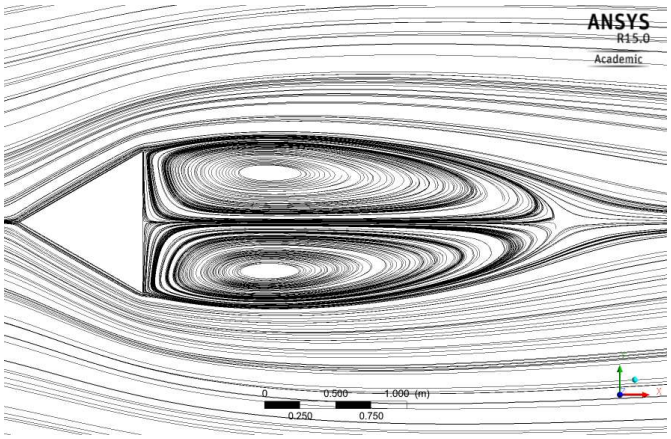

c)

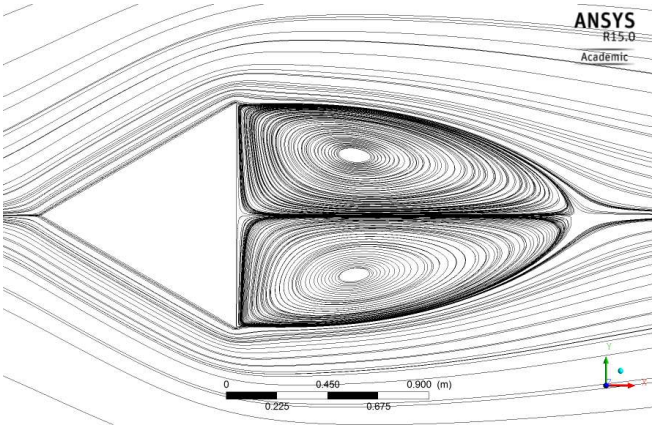

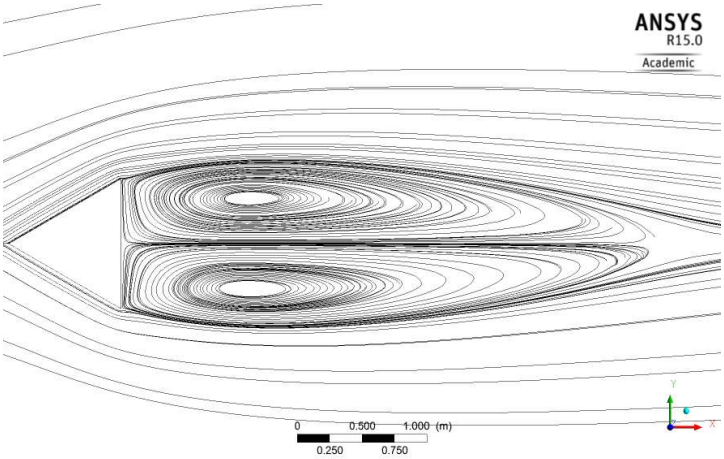

Fig. 4.3. (Continued)

Table 4.1. Values of Total Drag coefficient for Power-law fluid in case of vertex facing upstream.

Re	C_D					
	n = 0.2		*n = 1*		*n = 1.8*	
	Present	*Literature*[9]	*Present*	*Literature*[9]	*Present*	*Literature*[9]
10	2.8992	3.1076	2.7953	2.7763	2.6741	3.597
20	1.7907	-	2.0199	2.01	2.1201	2.704
25	1.575	-	1.8354	-	1.9723	-
30	1.4302	-	1.7018	1.693	1.8621	2.316
40	1.2457	-	1.1517	-	1.7008	-

Table 4.2. Values of Pressure Drag coefficient for Power-law fluid in case of vertex facing upstream.

Re	C_{DP}					
	n = 0.2		*n = 1*		*n = 1.8*	
	Present	*Literature*[9]	*Present*	*Literature*[9]	*Present*	*Literature*[9]
10	2.2409	2.4112	1.4551	1.3686	1.1325	1.082
20	1.4297	-	1.0961	1.071	0.9354	0.899
25	1.2786	-	1.0189	-	0.8878	-
30	1.1781	-	0.9651	0.9433	0.853	0.822
40	1.0504	-	0.8929	-	0.8039	-

Table 4.3. Values of Recirculation Length for Power-law fluid in case of vertex facing upstream.

Re	L_R		
	n = 0.2	*n = 1*	*n = 1.8*
10	0.5415	0.8385	1.5101
20	1.3557	1.4961	2.4525
25	1.8162	1.8987	2.9345
30	2.2923	2.2923	3.4620
40	3.2133	3.0000	4.2728

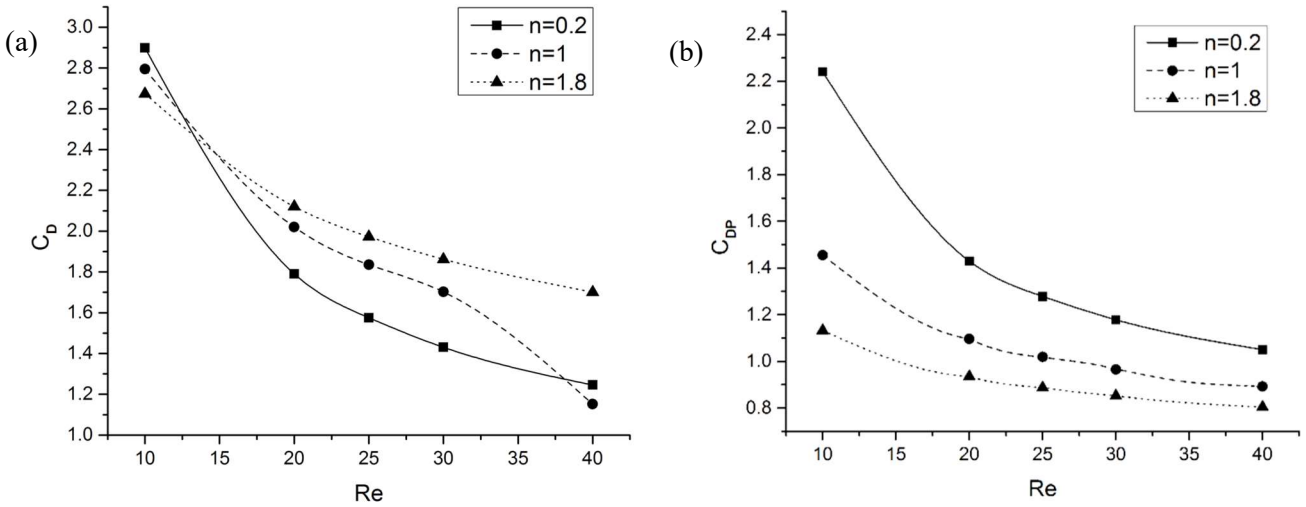

Fig. 4.4. Variation of (a) Total Drag coefficient, (b) Pressure Drag coefficient, and (c) Recirculation Length with Reynolds number, for n=0.2, 1 and 1.8.

(c)

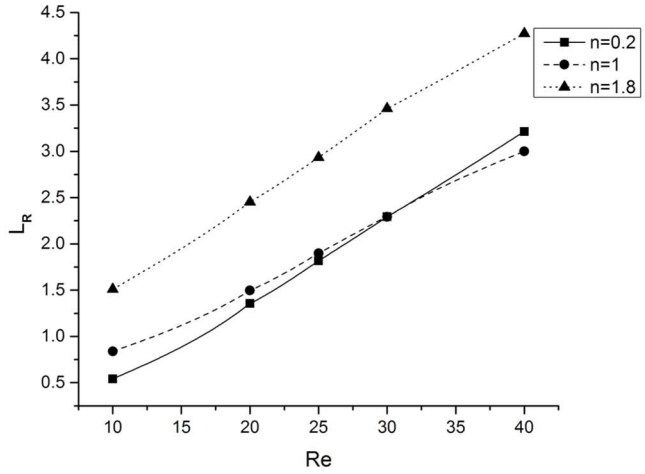

Fig. 4.4. (Continued)

4.2.2 Vertex Facing Downstream

a)

b)

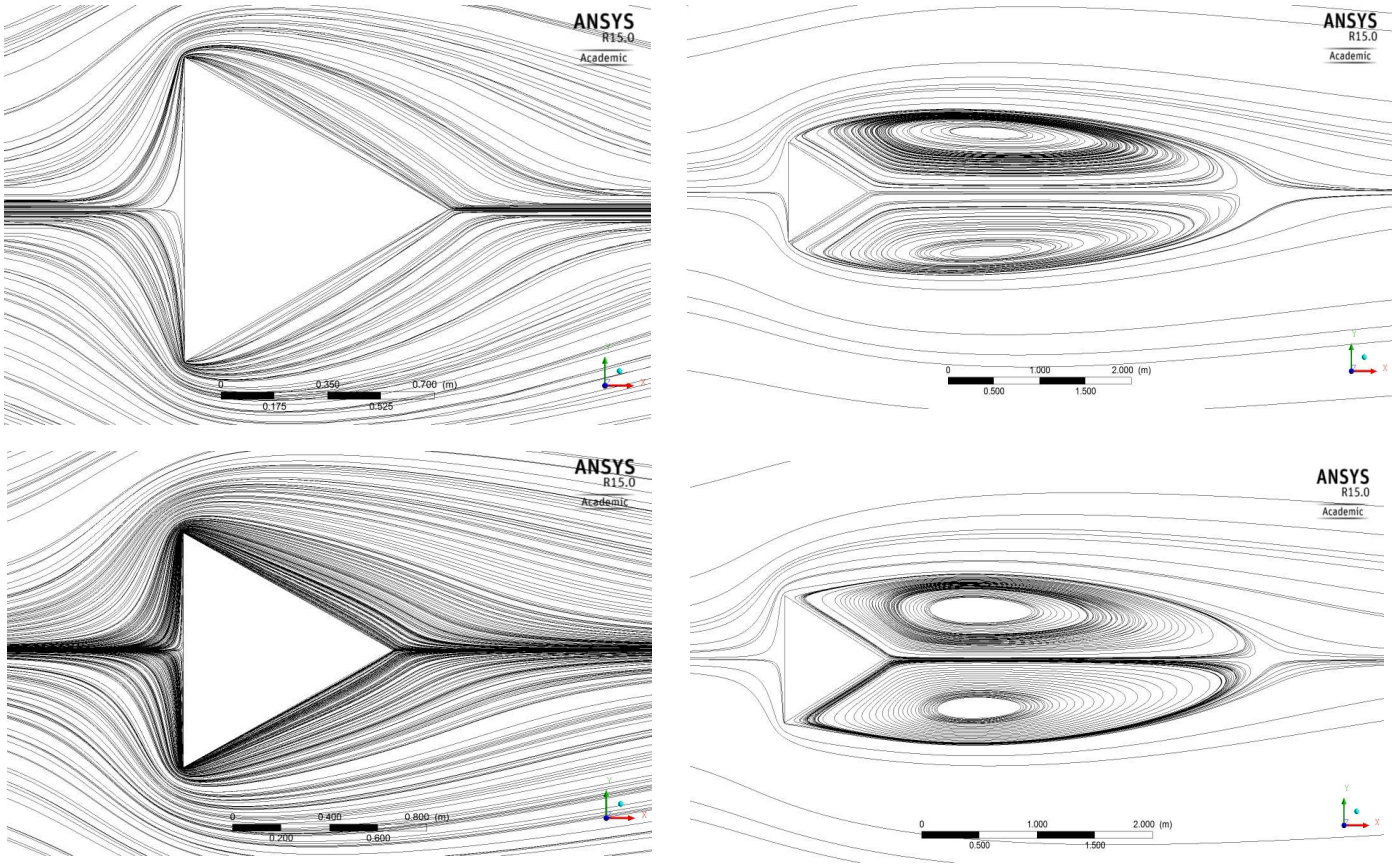

Fig. 4.5. Streamline patterns, in case of vertex facing downstream, for Reynolds number 10(left) and 40(right), and power-law index; a) n=0.2, b) n=1, c) n=1.8.

c)

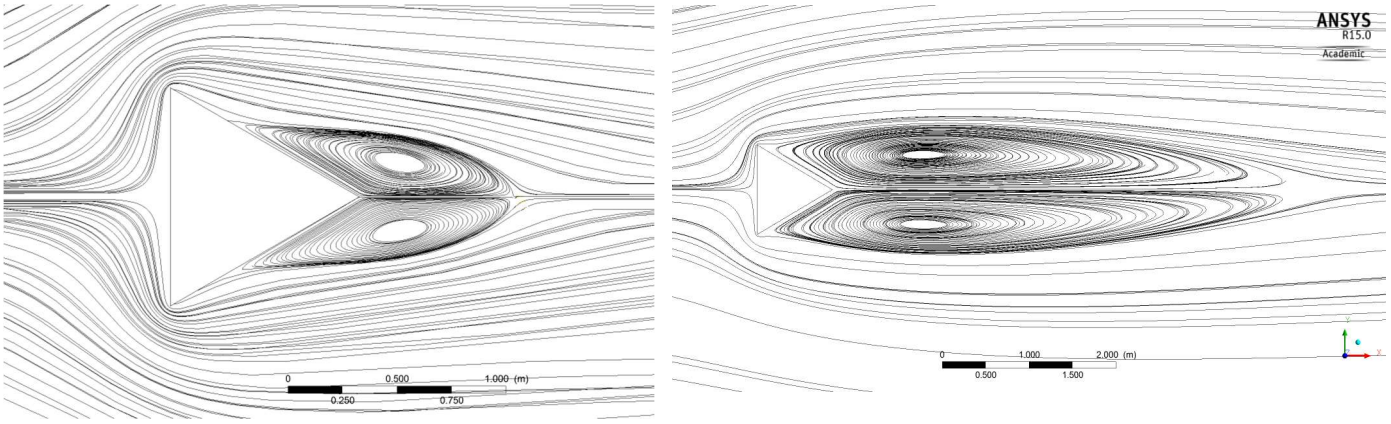

Fig. 4.5. (Continued)

Table 4.4. Values of Total Drag coefficient for Power-law fluid in case of vertex facing downstream.

Re	C_D					
	n = 0.2		*n = 1*		*n = 1.8*	
	Present	*Literature*[9]	*Present*	*Literature*[9]	*Present*	*Literature*[9]
10	2.8992	3.1076	2.7953	2.7763	2.6741	3.597
20	1.7907	-	2.0199	2.01	2.1201	2.704
25	1.575	-	1.8354	-	1.9723	-
30	1.4302	-	1.7018	1.693	1.8621	2.316
40	1.2457	-	1.1517	-	1.7008	-

Table 4.5. Values of Pressure Drag coefficient for Power-law fluid in case of vertex facing downstream.

Re	C_{DP}					
	n = 0.2		*n = 1*		*n = 1.8*	
	Present	*Literature*[9]	*Present*	*Literature*[9]	*Present*	*Literature*[9]
10	3.156	3.3699	2.8086	2.818	2.681	2.818
20	2.0096	-	2.1062	2.116	2.1932	2.021
25	1.844	-	1.9457	-	2.0634	-
30	1.746	-	1.832	-	1.9649	1.967
40	1.6161	-	1.6766	-	1.8193	-

Table 4.6. Values of Recirculation Length for Power-law fluid in case of vertex facing downstream.

Re	L_R		
	n = 0.2	*n = 1*	*n = 1.8*
10	-	-	1.6099
20	1.3159	1.7055	3.0895
25	2.3407	2.25703	3.8699
30	3.2096	2.8649	4.6001
40	4.9998	4.1441	6.2958

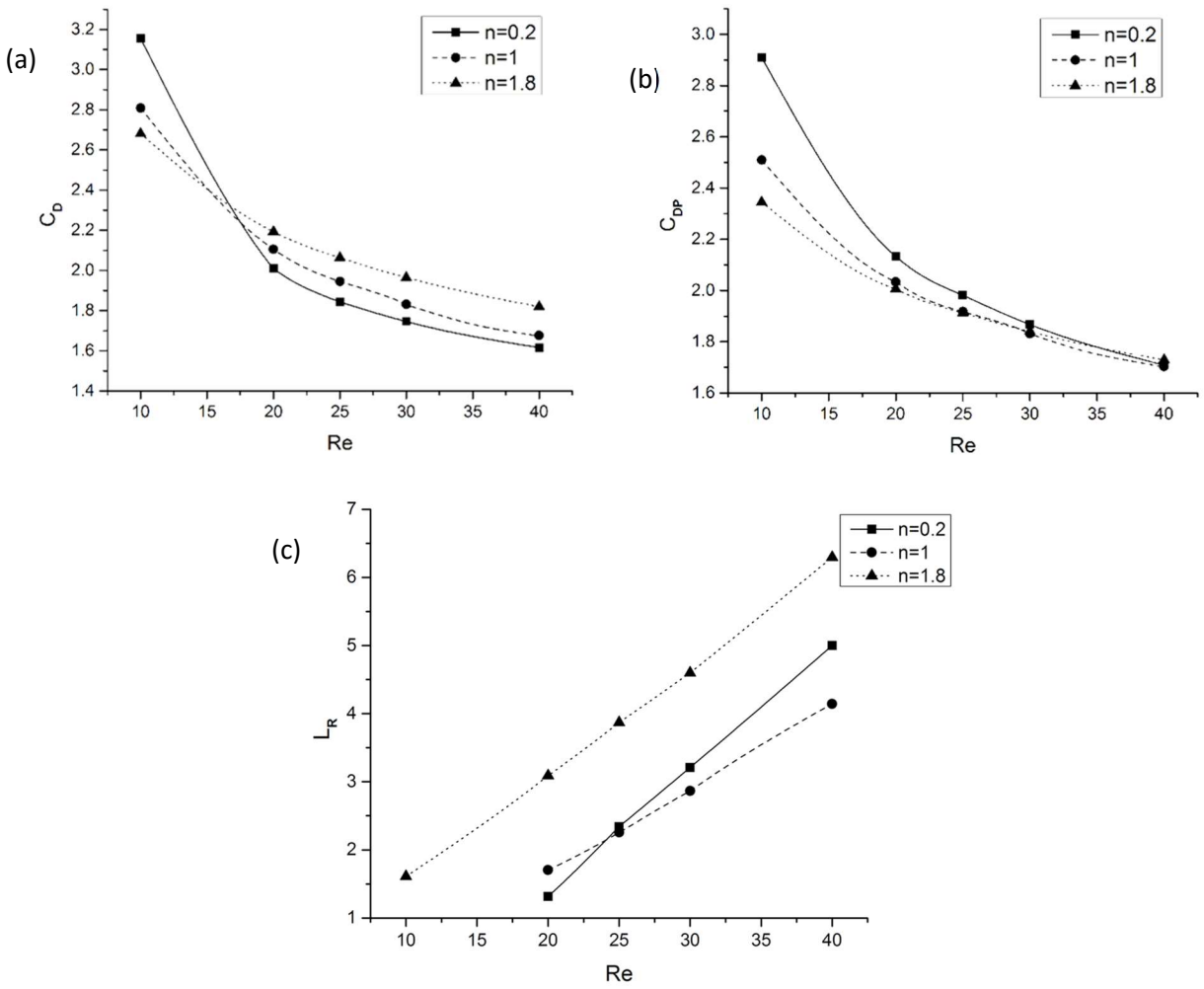

Fig. 4.6. Variation of (a) Total Drag coefficient, (b) Pressure Drag coefficient, and (c) Recirculation Length, with Reynolds number, for n=0.2, 1 and 1.8.

If we consider experimental procedures, the flow may become unstable due to several factors such as non-uniform flow conditions, absurdness in the physical boundaries, vibrations produced by mechanical devices like pumps or compressors, surface roughness, and several other factors that are irrelevant for numerical simulations. Whereas, even with symmetric initial and boundary conditions, the rounding off, truncation, and discretization errors are some of the factors which may ultimately destabilize the flow and thereby directed towards the vortex-shedding regime under adequate conditions of Reynolds number. Prioritizing the presentation of results obtained, the validation of the numerical methodology used here, is mandatory.

The results obtained here, and the literature values for Power-law fluid flow past an equilateral triangle, are compared in terms of total drag coefficient, pressure drag coefficient and recirculation length for the values of Power-law Index and Reynolds number, considered here.

When the fluid approaches the triangular cylinder, its velocity approaches zero on reaching the front stagnation point, and after that it moves about the surface of the cylinder. At a low value of Reynolds number, the fluid momentum is minute and hence an element of fluid is able to follow closely the surface of the cylinder. However, as the value of Reynolds number is increased progressively, the fluid momentum increases and hence the stabilizing viscous forces decreases. As a result, at a critical value of Reynolds number, this leads to the production of adverse eddy motions in form of pressure gradients over the surface of the cylinder. And this be the reason for the separation of flow from the surface of the cylinder.

Fig. 4.3 and 4.5 demonstrate the streamline patterns around the submerged cylinder for extreme values of Reynolds number (Re= 10 and 40, for both the orientations) and power-law index (n = 0.2, 1 and 1.8). In these figures, for a low Power-law index value, the flow around the cylinder is not/barely separated at Reynolds number 10(left column), while at Reynolds number 40(right column), quite distinctive separation is seen to have occurred over the edge of the triangular cylinder.

Fig. 4.4(a), 4.4(b), 4.6(a) and 4.6(b) show that for both the orientation of the triangle, the total drag coefficient and the pressure drag coefficient exhibit an inverse dependence upon Reynolds number, for the set of conditions investigated herein. Furthermore, the total and pressure drag coefficients for the cylinder with its apex facing downstream have a little higher value as compared to that for the apex facing upstream direction, for a certain fixed value of Reynolds number. The variation between the two values is of the order (10^{-2}) at a low value of Reynolds numbers, which further increases with increasing Reynolds number. This variation is simply because of the fact that at a low value of Reynolds number the elements of the fluid are able to follow closely across the surface of the cylinder, while for a higher Reynolds number the flow separation cause a lower drag value.

Fig. 4.4(c) and 4.6(c) show that for both the orientation of the triangle, the recirculation length increases as the Reynolds number increases in the set of conditions studied herein.

Chapter 5

Conclusions

The dependence of the appearance of wakes and the initiation of vortex shedding, on the power-law index and Reynolds number, has been examined numerically for the flow past an equilateral triangular cylinder, in laminar flow regime. For both the orientations of the cylinder, the wake separation and vortex shedding phenomena are found to be delayed as the behavior of the fluid flow changes from shear-thinning to Newtonian, and finally to shear-thickening. In the laminar flow regime, the total drag coefficient and the pressure drag coefficient values decrease with Reynolds number for any fixed value of power-law index. With increase in the Reynolds number value, the dependence on Power-law index eventually diminishes.

The results obtained in the present work for the different parameters such as drag coefficient, pressure drag coefficient, streamlines, recirculation length are found to be in good agreement with the literature values for the Power-law fluid flow past an equilateral triangular cylinder[9].

Bibliography

[1] Warren L. McCabe, Julian C. Smith, Peter Harriott, *Unit Operations of Chemical Engineering*, Seventh Edition, International Edition(2005), McGraw-Hill Education(Asia), p. 159.

[2] U Ghia, K.N Ghia and C.T Shin, *High Re solutions for incompressible flow using the Navier-Stokes equation and Multi-grid method* , University of Cincinnati, Cincinnati, Ohio(1982) 45221.

[3] C.P. Jackson, *A finite-element study of the onset of vortex shedding in flow past variously shaped bodies*, J. Fluid Mech. 182 (1987) 23-45.

[4] B.J. Zielinska, J.E. Wesfreid, *On the spatial structure of global modes in wake flow*, Phys. Fluids 7 (1995) 1418-1424.

[5] H. Abbassi, S. Turki, S.N. Nasrallah, *Numerical investigation of forced convection in a plane channel with a built-in triangular prism*, Int. J. Therm. Sci. 40 (2001) 649-658.

[6] A.K. De, A. Dalal, *Numerical simulation of unrestrained flow past a triangular cylinder*, Int. J. Num. Meth. Fluids 52 (2006) 801-821.

[7] Z. Faruquee, T.V. Olatunji, *Steady and unsteady laminar flow past an equilateral triangular cylinder for two different orientations*, Proceedings of 5th joint ASME/JSME fluids engineering conference, San Diego, USA(2007) 1445-1450.

[8] S. Srikanth, A.K. Dhiman, S. Bijjam, *Incarcerated flow and heat transfer across a triangular cylinder in a channel*, Int. J. Therm. Sci. 49 (2010) 2191-2200.

[9] A. Prhashanna, A.K. Sahu, R.P. Chhabra, *Flow of power-law fluids past an equilateral triangular cylinder: momentum and heat transfer characteristics*, Int. J. Thermal Sci. 50 (2011) 2027-2041.